U.P.B. Sci. Bull., Series D, Vol. 88, Iss. 3, 2026 ISSN 1454-2358

DYNAMIC PARAMETER ANALYSIS AND STRUCTURAL DESIGN OF A PENDULUM-DRIVEN SPHERICAL ROBOT FOR PIPELINE INSPECTION

Yue CUI[1*], Fangyuan MAO[2], Silin LAN[3], Nan LIN[4], Huijie HAN[5], Yifan SUN[6]

The spherical robot, characterized by its simple mechanical structure, agile steering, and robust autonomous control capability, holds promising potential for industrial pipeline inspection. This study focuses on the analysis of dynamic parameters and the structural design of a pendulum-driven spherical robot. By examining the force and moment balance between the spherical shell and the internal pendulum, a dynamic model for the robot's linear rolling motion was established. Dynamic simulations were conducted to evaluate the influence of key parameters—including pendulum mass, angular velocity, and rod length—on the robot's rolling behavior. Results indicate that during straight-line rolling, the robot's velocity, friction with the pipeline inner wall, motor torque, and pendulum angle exhibit sinusoidal variations. Increases in pendulum mass and rod length raise the frequency of velocity fluctuations, while higher pendulum rotational speed amplifies the rolling velocity amplitude. Following theoretical analysis, a complete prototype was designed and subjected to motion tests. Experimental trajectories aligned well with simulation outcomes, confirming the robot's stable and controllable motion performance. Through integrated theoretical modeling, parameter optimization, structural design, and experimental validation, this study develops a spherical robot capable of meeting the demands of small-diameter pipeline inspection tasks, demonstrating its practical applicability and motion reliability.

Keywords: spherical robot; structural design; dynamic simulation; control; experiment.

1. Introduction

With the increasing demand for urban gas energy, transportation pipelines have become one of the most important urban infrastructure systems [1]. Due to

[1*] Associate Professor, Hebei Key of Laboratory of Intelligence Equipment Digitalize Design and Process Simulation, Tangshan University, Tangshan 063000, China; e-mail: cuiyue@tsc.edu.cn
[2] Tangshan Research Institute of Beijing Jiaotong University, Tangshan 063000, China; e-mail: 21121398@bjtu.edu.cn
[3] College of Science, Beijing University of Civil Engineering and Architecture, Beijing 102627, China; e-mail: 202409010116@stu.bucea.edu.cn
[4] Senior Engineer, China Special Equipment Inspection and Research Institute, Beijing 100029, China; e-mail: sy_linnan@163.com
[5] Senior Engineer, Tangshan Metallurgical Saw Blade Co., Ltd., Tangshan 063020, China; e-mail: 603010204@163.com
[6] Hebei Key of Laboratory of Intelligence Equipment Digitalize Design and Process Simulation, Tangshan University, Tangshan 063000, China; e-mail: 794703392@qq.com
*Corresponding author: Yue Cui

the inevitable aging, corrosion, and other factors caused by the service environment and long-term use, leakage or even explosion caused by pipeline rupture can lead to serious safety accidents [2]. The manual inspection of pipelines has disadvantages such as high inspection costs and longtime consumption. Pipeline inspection robots overcome these manual inspection drawbacks and are increasingly being used as an effective inspection solution [3,4].

Pipeline inspection robots are electromechanical integrated systems that integrates mechanical structure, inspection system, control system, and signal transmission system [5]. They integrate various sensors such as ultrasonic, infrared, and visual sensors to achieve pipeline inspection during the movement process [6]. Through remote control by inspection personnel or automatic control by computers, climbing and moving within narrow and complex transportation pipelines can be achieved for tasks such as fault detection and precise positioning [7]. Heesik et al [8] developed a modularized autonomous pipeline inspection robot which was aimed at inspect in-service urban gas pipelines with a diameter of 200 mm. Chan et al. [9] proposed a portable and automatic robot which exhibited superior capacities in complicated pipe environments for turning into 90° elbows, that can be applied to any pipeline system. Wang et al. [10] proposed a spanning and bending pipeline inclination measurement based on an in-pipe spherical detector, and carried out experiments to verify. Huang et al. [11] obtained an absolute localization error by using spherical detector through 3D rotation. Adam et al. [12] designed a pipe robot prototype based on a vertebra concept with the localization algorithm which track the progress of the robot inside the tubes. Abe [13] conducted stops and remote morphological deformation experiments to confirm the operation of the spherical shell robot during rolling. Li and Guo [14] proposed a new attitude regulator based on the counterweight mechanism to perceive and regulate the attitude of the spherical underwater robot.

According to the analysis of the research status, one class of the driving system of spherical robots generates torque by changing the overall center of mass position to promote the rolling and turning of the robot; another type was based on the law of conservation of angular momentum, which keeps the center of mass of a spherical robot at the center of the sphere [15], and the robot obtains a torque opposite to the driving direction to make the sphere roll. Spherical robots are generally non-linear, under-actuated, and strongly coupled non-holonomic systems [16]. An et al. [17] presented an uncertain moving obstacle avoiding method based on the improved velocity obstacle method for spherical underwater robot. Montenegro et al. [18] developed a model of a spherical robot which and has a single point of support in the CoppeliaSim simulator. Haribabu and Pathak [19] developed a pipe inspection robot which has four adjustable arms equipped with a wheel for forward movement along the pipe wall.

In order to design and use a structurally simple and highly reliable internal inspection robot in the pipeline inspection environment, the pendulum-driven spherical robot was selected, by use of a pendulum as the power source for the spherical robot, combined with control systems such as microcontrollers and distance sensors, completed the robot's walking and turning function inside the pipeline. Compared with other types of pipeline inspection robots, the pendulum-driven spherical robot structure was relatively simple. Choosing PVC material for 3D printing can reduced processing costs and shorten production cycles, and facilitated the optimization and upgrading of physical prototypes in the later stage. Unlike most human controlled pipeline inspection robots, the pendulum-driven spherical robot can achieved autonomous recognition and controlled without the need for external cables or other external hardware systems, reduced the workload of inspection personnel. By compare with the simulation outcomes and linear walking experiments, demonstrating that the robot exhibits reliable and effective motion performance.

2. Analysis of kinematics and dynamics

Through the integration of theoretical analysis, structural design, simulation, and experimental validation, a pipeline inspection spherical robot with steering function was developed. The overall mechanical structure of the spherical robot was primarily decomposed into two components: the spherical shell, which serves a load-bearing function, and the internal mechanism responsible for motion control. Under the assumption of a uniformly distributed mass of the spherical shell, the center of mass of the shell remains coincident with the geometric center of the sphere and remains stationary during motion. The rotation of the motor induces pendulum motion about the center, generating a gravitational torque that propels the sphere [20]. To facilitate analysis of the sphere's motion, the mass of the internal structure was treated as an equivalent pendulum. A dynamic coordinate system *XYZ* was established with the geometric center O_1 of the sphere as the origin, as illustrated in Fig. 1 (where the upper and lower horizontal lines represent the pipeline wall).

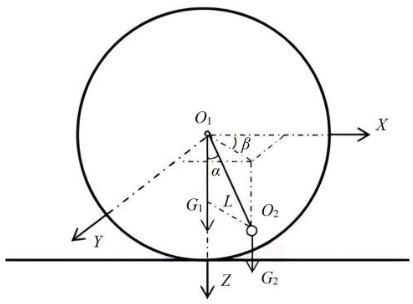

Fig. 1 The dynamic coordinate system of the spherical robot

Let the weight of the robot's spherical shell be G_1, and that of the internal structural weight be G_2 with its center of mass located at O_2. The center of the sphere gravity was at any position in space and the length of the line connecting it to the center O_1 was L. The angle between the line O_1O_2 and the vertical direction was α, and the angle between its projection on the plane XO_1Y and the horizontal axis O_1X was β. The position of the center of mass O_2 was represented by the spatial vector $\overrightarrow{O_1O_2}$:

$$\overrightarrow{O_1O_2} = (L\sin\alpha\cos\beta,\ L\sin\alpha\sin\beta,\ L\cos\alpha) \tag{1}$$

The coordinate position of the centroid of the internal structure can be expressed by the components of the weight on each axis:

$$\begin{bmatrix} X_{O_2} \\ Y_{O_2} \\ Z_{O_2} \end{bmatrix} = G_2\left[L\sin\alpha\cos\beta,\ L\sin\alpha\sin\beta,\ L\cos\alpha\right]^T \tag{2}$$

Thus, the centroid of the spherical robot in the spatial coordinate system is given by:

$$\begin{cases} X_O = \dfrac{G_1\cdot 0 + G_2 L\sin\alpha\cos\beta}{G_1+G_2} = \dfrac{G_2}{G_1+G_2}L\sin\alpha\cos\beta \\ Y_O = \dfrac{G_1\cdot 0 + G_2 L\sin\alpha\sin\beta}{G_1+G_2} = \dfrac{G_2}{G_1+G_2}L\sin\alpha\sin\beta \\ Z_O = \dfrac{G_1\cdot 0 + G_2 L\cos\alpha}{G_1+G_2} = \dfrac{G_2}{G_1+G_2}L\cos\alpha \end{cases} \tag{3}$$

The pivotal factor influencing the centroid position is the ratio between G_1 and G_2. When G_1 takes is substantially larger than G_2, all three components decrease, indicating that the system's centroid approaches the geometric center.

Prior to rolling, the spherical robot is in a state of static equilibrium [21]. The internal structure must supply a torque sufficient to overcome the rolling friction torque. The static equilibrium condition is expressed by equation (4):

$$G_2\cdot L\sin\alpha \le R\cdot f \Rightarrow \sin\alpha \le \frac{Rf}{LG_2} \Rightarrow \alpha \le \arcsin\frac{Rf}{LG_2} \tag{4}$$

Assuming the horizontal distance from the center of mass O_2 to the axis of rotation is d:

$$d \ge L\times\cos\alpha = L\times\cos(\arcsin\frac{Rf}{LG_2}) \tag{5}$$

Where, R represents the maximum radius of the sphere, and f denotes the rolling friction force. Given a coefficient of friction μ at the pipeline base:

$$f = \mu \cdot G = \mu \cdot (G_1 + G_2) \tag{6}$$

Using inverse trigonometric relations, it follows that:

$$\cos(\arcsin\frac{Rf}{LG_2}) = \sqrt{1-(\frac{Rf}{LG_2})^2} = \frac{\sqrt{L^2 G_2{}^2 - R^2 f^2}}{LG_2} \tag{7}$$

Substituting equations (6) and (7) into equation (5) yields the critical centroid position for static equilibrium:

$$d = \frac{\sqrt{(L^2 - \mu^2 R^2)G_2{}^2 - \mu^2 R^2 (G_1{}^2 + 2G_1 G_2)}}{G_2} \tag{8}$$

The spherical robot was simplified into a two-dimensional model comprising the spherical shell and the pendulum. The interaction between these components and the sphere's motion was examined. The simplified planar model is depicted in Fig. 2.

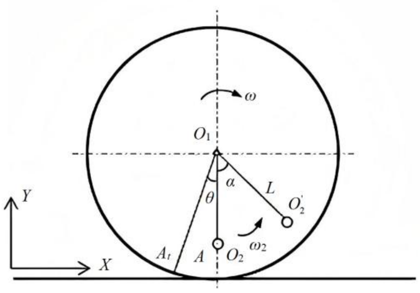

Fig. 2 the planar model of the spherical robot

In the initial state, the pendulum hangs vertically downward, with the contact point labeled A. After time t, the sphere rotates, moving contact point A to A_t. The rotation angle of the sphere's center is denoted as θ. τ is the driving torque of the motor. As the connecting rod rotates from OO_2 to $OO_2{}'$, the pendulum swings by an angle α. Let the coordinates of the sphere's center be $O(x_1, y_1)$ and those of the pendulum's center be $O_2(x_2, y_2)$.

The dynamic model of the spherical robot is derived using the Lagrangian equation. By calculating the kinetic energy of the spherical shell and the pendulum, the system's kinetic energy is obtained as:

$$K = \frac{1}{2}J_1\dot{\theta}^2 + \frac{1}{2}J_2\dot{\alpha}^2 + m_c rL\dot{\theta}\dot{\alpha}\cos\alpha \tag{9}$$

Where,

$$J_1 = (m_s + m_c)r^2 + I_s \tag{10}$$

$$J_2 = m_c L^2 + I_c \tag{11}$$

The shell mass is equivalent to m_s, with a moment of inertia of I_s; the pendulum mass is equivalent to m_c, with a moment of inertia of I_c. Selecting the horizontal plane as the zero potential energy surface, the potential energy of the spherical robot system is:

$$\mathrm{V} = (m_s + m_c)gr - m_c gL\cos\alpha \tag{12}$$

By substituting the Lagrange function L=K-V into the Lagrange equation, the dynamic model of the spherical robot can be obtained:

$$J_1\ddot{\theta} + m_c rL\ddot{\alpha}\cos\alpha - m_c rL\dot{\alpha}^2\sin\alpha = \tau \tag{13}$$

$$J_2\ddot{\theta} + m_c rL\ddot{\alpha}\cos\alpha + m_c rL\sin\alpha = \tau \tag{14}$$

In equation(13)-(14), the angular acceleration of the spherical shell is influenced not only by its own mass and the sphere's radius but also by factors such as the pendulum mass and the connecting rod length. Larger shell and pendulum masses, a larger sphere radius, a shorter connecting rod, and greater motor torque contribute to increased angular acceleration of the shell. The angular acceleration of the pendulum is affected by its mass, the rod length, and the motor torque. A larger torque, smaller pendulum mass, and shorter rod result in higher pendulum angular acceleration. Therefore, in the design of a spherical robot, the pendulum mass and connecting rod length should be optimized to achieve high rolling speed without compromising kinematic performance.

By analyzing the positional conditions that the center of mass of the spherical robot must satisfy when it is in static equilibrium within the pipeline, the velocity and influencing factors of the spherical robot during motion can be obtained, verifying that it is an underactuated nonholonomic system. Through analyzing the moment equilibrium between the spherical shell and the pendulum, a dynamic model for the spherical robot's movement within the pipeline is derived, providing a theoretical basis for mechanical structure design.

3. Structural design and motion simulation

3.1 Structural design

The overall architecture of the spherical robot comprises two main subsystems: the mechanical structure and the control structure. The mechanical structure provides structural support for the robot's motion and accommodates hardware such as cameras and sensors to facilitate the execution of various operational tasks. The control structure serves as the driving unit of the robot, directly influencing its motion performance. A schematic of the pendulum-driven spherical robot is illustrated in Fig. 3. The control system receives signals and completes the control of the mechanical system, achieving linear motion and steering.

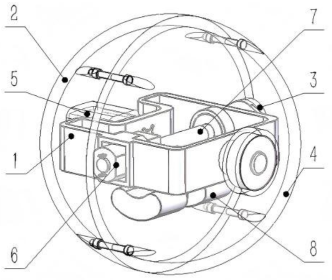

(1. Bracket, 2. Upper ball shell, 3. Distance measuring sensor, 4. Lower ball shell, 5. Motor 1, 6. Motor 2, 7. Short shaft, 8. Pendulum)
Fig. 3 Schematic diagram of spherical robot structure

Linear motion and turning are achieved by controlling two mutually perpendicular drive motors to adjust the position of the pendulum's center of gravity. Motion is initiated when the gravitational torque generated by the pendulum exceeds the frictional torque acting on the robot at the pipeline surface. Motor 1 is mounted within the base of the upper hemispherical shell, with its output shaft connected to a D-shaped gear. This gear is interference-fitted into a geared hole on the bracket, while the opposite end of the bracket is connected to the lower hemispherical shell via a bearing. Motor 2 is secured directly into a rectangular slot on the bracket, with its output coupled to a short shaft and the counterweight (pendulum mass). The other end of the short shaft is supported by the bracket through a bearing.

The total mass of the spherical robot is 0.612kg. When the pendulum is oriented vertically, the vertical distance between the sphere's center of gravity and the XY plane is 18.664 mm, and its offset from the Z-axis is 0.652 mm. The internal layout is compact, with a spatially uniform mass distribution.

3.2 Dynamics simulation model and motion parameter analysis

A dynamic model of the spherical robot was developed using virtual prototyping technology in ADAMS (Fig.4), incorporating a contact collision model [22].

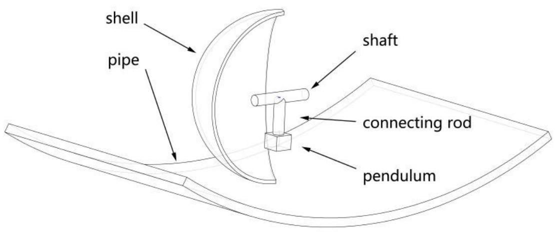

Fig.4 Spherical robot model in ADAMS

In Fig.4, the shell is connected to the pipe through a contact pair, limiting the degree of freedom to 1; the shaft is connected to the shell through a rotational pair, limiting the degree of freedom to 5; the connecting rod is connected to the shaft through a fixed pair, limiting the degree of freedom to 6; the pendulum is connected to the rod through a fixed pair, limiting the degree of freedom to 6; the pipe is connected to the ground through a fixed pair, limiting the degree of freedom to 6. The contact force parameters are listed in Table1.

Table 1

Contact force parameter setting

Parameters	Symbol	Numerical value (unit)
stiffness	k	10^5(N/mm)
force index	n	2.2
damping	c	100(N·s/mm)
penetration depth	d	0.1(mm)
static friction coefficient	μ_s	0.3
dynamic friction coefficient	μ_d	0.1
Static translational velocity	v_s	1mm/s

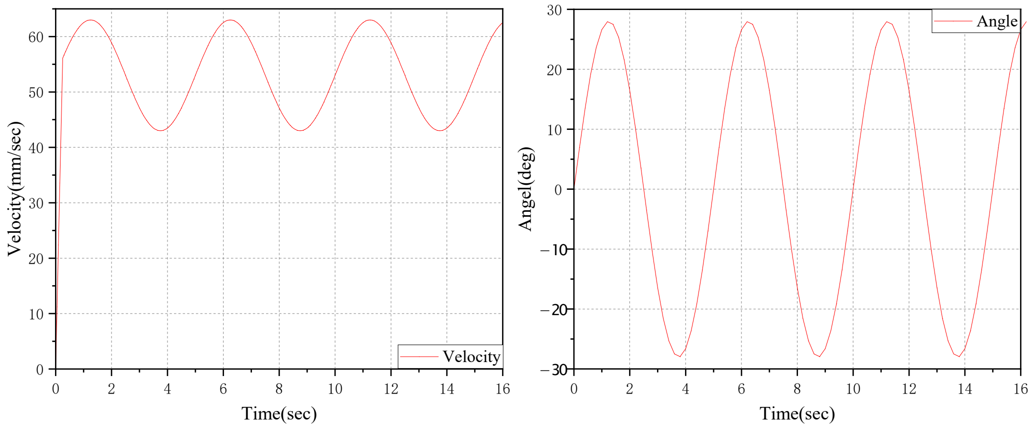

(a) Velocity of spherical robot (mm/sec) (b) Pendulum rod angle change curve (°)

Fig. 5 Curve of velocity and pendulum rod angle variation of spherical robot

Time-varying curves of the rolling speed and pendulum angle of the spherical robot are presented in Fig.5. Under a time-varying motor drive function, the rolling velocity exhibits sinusoidal oscillations, as shown in Fig. 5a. Due to sliding friction, the initial velocity increases nearly linearly. After stabilization, the velocity fluctuates sinusoidally with an average value of 52 mm/s and a peak value of 62 mm/s. As illustrated in Fig. 5b, the pendulum angle increases during acceleration phases, ranging in amplitude from –28° to 28°. A larger pendulum angle corresponds to a greater gravitational torque, shifting the sphere's center of mass toward the front of the internal space. During deceleration, the pendulum angle decreases, relocating the center of mass toward the rear.

3.3 Analysis of factors influencing the rolling speed of spherical robot

A controlled-variable approach was employed to investigate the effects of pendulum mass, pendulum length, and pendulum angular velocity on the rolling speed of the spherical robot (Fig.6). Initially, with the pendulum length and angular velocity held constant, the rolling speed under different pendulum masses was obtained, as shown in Fig. 6a. Next, with the pendulum length and mass kept unchanged, variations in the pendulum angular velocity yielded the velocity results illustrated in Fig. 6b. Finally, by maintaining constant pendulum mass and angular velocity while altering only the pendulum length, the corresponding rolling speeds were documented in Fig. 6c.

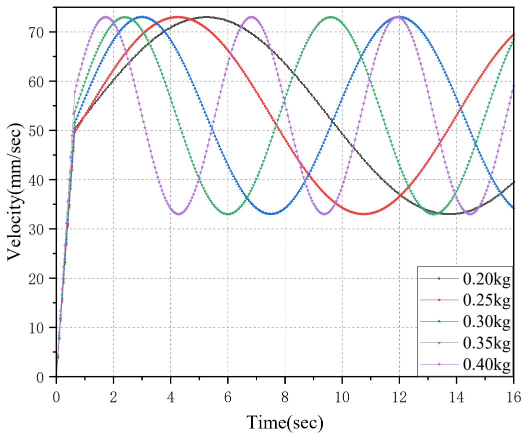

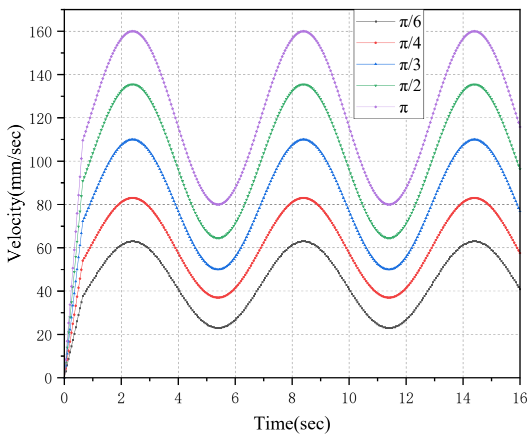

(a) Pendulum weight (kg) (b) Pendulum rod angular velocity (rad/s)

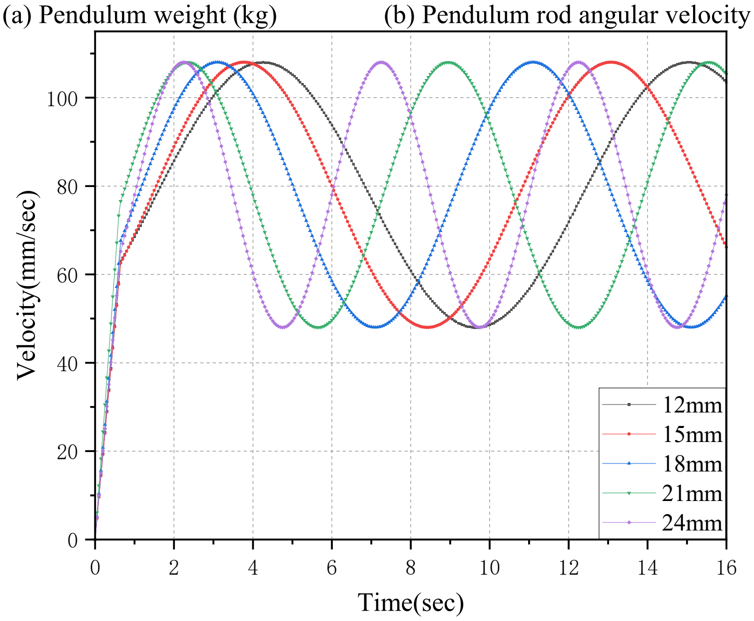

(c) Pendulum rod length (mm)

Fig.6 The influence of different factors on the rolling speed of spherical robot

As observed in Fig. 6a, as the pendulum mass increased from 0.2 kg to 0.4 kg, the period of oscillation in rolling speed decreased from 18 s to approximately 2 s, and the frequency of speed variation increased accordingly. Altering the pendulum mass affected the frequency of speed fluctuation but not its amplitude. According to Fig. 6b, when the angular velocity of the pendulum rod was increased from π/6 rad/s to π rad/s, the average rolling speed of the sphere decreased, while the amplitude of speed variation increased from 40 mm/s to 80 mm/s. A smaller angular velocity resulted in a more stable speed profile. Variations in angular velocity did not influence the frequency of speed oscillations, with the period remaining constant at 6 s. As shown in Fig.6c, increasing the pendulum length from 12 mm to 24 mm led to a higher frequency of speed variation, without affecting the amplitude of the speed. Longer pendulum lengths correspond to faster fluctuations in rolling speed.

In summary, the selection of pendulum mass and length is directly linked to the required motor output torque. Considering the constrained internal space of the spherical robot and the need for stable velocity profiles and long-distance operation, a prototype was fabricated with a pendulum length of 18 mm and a pendulum mass of 0.2 kg for subsequent experimental validation.

4. Prototype and walking experiment of spherical robot

Although there were many mechanical materials that can fully satisfied the structural performance of spherical shell, the processing cost was high and the time cost was long. PVC has stable physical properties and good mechanical properties, and can be used as an electrical insulator. The spherical shell was constructed from PVC material. At the same time, 3D printing technology was used to develop experimental physical prototypes, which can reduce the production cycle and adjust problems in a timely manner, saving costs and experimental time. A ZGA12 stepper motor was selected for actuation(Table 2), driven by an L298N motor driver module. The control system was built around an ATmega328P microcontroller. A PID closed-loop control strategy was implemented, and the simulation structure is illustrated in Fig. 7.

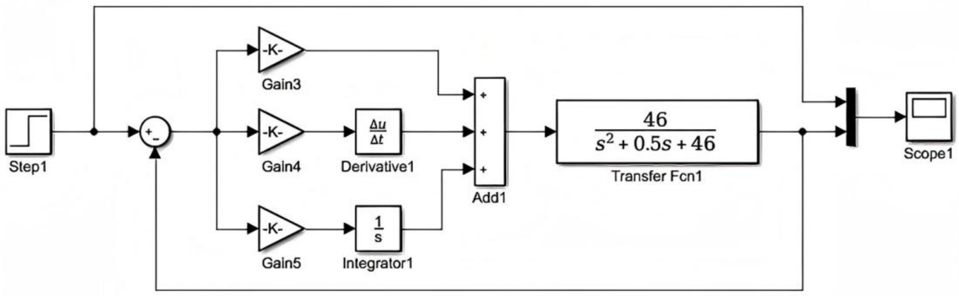

Fig. 7 PID structure diagram of spherical robot

The ZGA12 stepper motor had a total body length of 22mm and a width of 12mm. Some parameters were shown in Table 2.

Table 2

Parameters of stepper motor ZGA12

Parameters	Body length	step angle	static torque	resistance	voltage	inductance
unit	*mm*	°	*kg·cm·min*	*Ω*	*V*	*mH*
value	22	1.8	15	4.9	2.45	1.7

The ATmega328P microcontroller control board included 12 digital input/output ports (TX, RX, D2~D13) and 8 analog input ports (A0~A7), 1 pair of TTL level serial transceiver ports RX/TX, and 6 PWM ports (D3, D5, D6, D9, D10, D11). L298N motor driver was select to amplify the signal power of the stepper motor, with a power supply voltage of 2V~10V, a size of 25 × 21 × 5mm, and a 15 pin package.

All structural components were manufactured using 3D printing technology. PVC material was selected for 3D printing, using Fused Deposition Modeling, with a layer height setting of 0.2mm, a printing speed of 40mm/s, and a nozzle temperature of 235 ℃. The prototype of the spherical robot was shown in Fig.8.

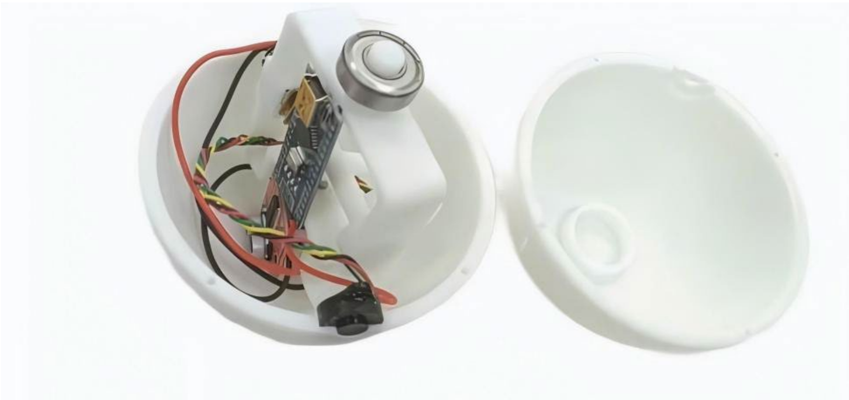

Fig. 8 Prototype of spherical robot

The key parameters of the spherical robot prototype were shown in Table 3.

Table 3

Main parameter settings of the spherical robot

Parameters	Symbol	Numerical value (unit)
The mass of the shell	m_1	0.15 (kg)
Radius of the spherical robot	R	45 (mm)
Pendulum mass	m_2	0.2 (kg)
Pendulum rod length	L	18 (mm)
motor torque	T	0.145 (N·m)
motor speed	n	4.5 (rad/s)

To quantitatively evaluate the linear locomotion capability of the spherical robot, the displacement components along three axes during motion were monitored in real time. A small displacement sensor was fixed at the center of the spherical robot, during the straight-line walking experiment, a camera was used to continuously capture images above the sphere, and the displacement components of the sphere collected by the sensor in the experimental results were represented in the form of a curve plot, as presented in Fig. 9.

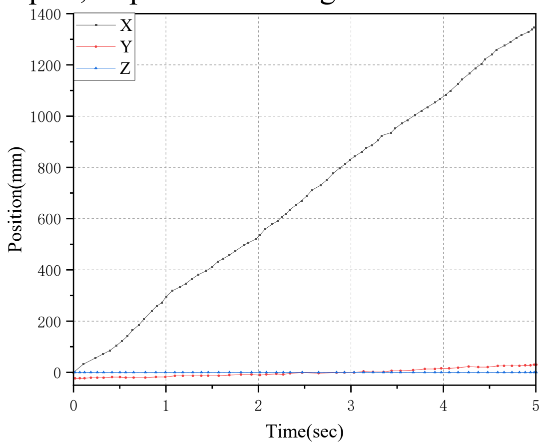

Fig. 9 Diagram of displacement experiment results

The experimental results indicate that the displacement components along the *Y*-axis and *Z*-axis were negligible during straight-line motion. The primary displacement occurred along the *X*-axis, demonstrating stable forward rolling. The velocity profile remained consistent, confirming that the robot exhibited straight-line rolling behavior. These findings validate the rationality of selecting a pendulum mass of 0.2 kg and a pendulum length of 18 mm based on prior simulations.

5. Conclusion

By combining theoretical analysis, structural design, simulation, and experiment, a spherical robot with simple structure and stable movement was developed to meet the requirements of small-diameter pipeline inspection work. By establishing the kinematic equations and dynamic simulation model of the spherical robot inside the pipeline, the influence of different pendulum masses, pendulum rod angular velocity, and pendulum rod lengths on the rolling of the sphere was obtained. The dynamic simulation analysis of the spherical robot showed that when the sphere rolls in a straight line, its rolling speed, friction force between the sphere and the inner wall of the pipeline, motor torque, and pendulum angle vary sinusoidally. The frequency of velocity fluctuations of the sphere was directly proportional to the pendulum mass and pendulum rod length, while the rotational speed of the pendulum determined the amplitude of the rolling velocity, showing a directly proportional relationship. The overall design of the pendulum-driven spherical robot was completed, and hardware selection as well as prototype fabrication and testing were carried out, including the integration of two motors, distance sensors, microcontrollers, and motor drive modules. A motor control system was established to directly regulate the angular velocity of the pendulum by adjusting motor speed. The prototype was successfully manufactured, and linear walking experiments were performed. Based on the experimental results, the trajectory of the spherical robot was compared with theoretical predictions and simulation outcomes, demonstrating that the robot exhibits reliable and effective motion performance.

The spherical robot designed in this article was limited to running in horizontal pipeline, and without considering the launch and recovery devices of the sphere in practical applications. In the next step of the work, a spherical robot that can move in the vertical direction would be designed, and a launch and recovery device for the sphere will be designed outside the pipeline. The leak detection module would be added inside the robot to meet the requirements of pipeline inspection tasks.

Acknowledgment

This research was funded by Science and Technology Innovation Program of Xiong'an New Area, Chinese Ministry of Science and Technology (Grant No. 2025XAGG0046).

REFERENCES

[1] *Qing-ran Ma, Qing-hua Chen, Jin-yin Liu et al.*, A review on related technologies of natural gas pipeline construction. Petrochemical Industry Technology, 2022, 29(4): 51-52.

[2] *Zhang-wei Ling, Cun-jian Miu, Ping Tang et al.,* Development of Research on Inner Inspection Robots and the Variable Diameter Technology in Industrial Pipelines. Welded Pipe and Tube, 2020, 43(3): 31-34, 40.

[3] *Peng-chao Chen, Yun-bin Ma, Bin Zhang et al.,* Construction and Development of Modern Pipeline Transportation System. Science and Technology Foresight, 2024, 3(02): 8-18.

[4] *Yao-feng Wu, Guan-nan Shi, Bin Guo et al.* Analysis of Several Scene Application of Oil and Gas Pipeline In-line Inspection Technology, China Special Equipment Safety. 2024, 40(10): 41-45+55.

[5] *Jiang-hong Sun, Yu-fan He, Jia-lin Wang, et al.,* Design of virtual simulation experimental system for pipeline testing robot. Experimental Technology and Management, 2021, 38(9): 138-142.

[6] *Zhan Qiang, Li Wei.,* Research Progress and Development Trend of Spherical Mobile Robots. Journal of Mechanical Engineering, 2019, 55(9): 1-17.

[7] *Glady Amen, Mohd Shahrimie, Mohamad Tarmizi et al.,* A review on soft in-pipe navigation robot from the perspective of material, structure, locomotion strategy, and actuation technique. Robotica, 2025, 43(1):387-413.

[8] *Jang Heesik, Kim Ho Moon, Lee Min Sub et al.,* Development of modularized in-pipe inspection robotic system: MRINSPECT VII+. Robotica, 2022, 40(5):1361-1384.

[9] *Chan Colin Pak Yu, Qu Zijia, Shiu Kin Hei et al*. In-Pipe Maintenance Robot Using Spray-In-Place Pipe Technique for Long-Distance and Complex Pipe Environment. Journal of Field Robotics, 2025, 42(4):1226-1243.

[10] *Wang Yuan, Wang Jialin, Ma Jinyu et al.* Subsea pipeline spanning detection using a spherical detector with AC magnetic proximity switches. Measurement, 2025, 244(28): 116475.

[11] *Huang Xinjing, Chen Shili, Guo Shixu, et al*. ,A 3D Localization Approach for Subsea Pipelines Using a Spherical Detector. IEEE Sensors Journal, 2017, 17(6): 1828-1836.

[12] *Cox Adam, Colaw Christopher, Richer Edmond et al.* Design and Static Equilibrium Analysis of a Modular Pipe Inspection Robot. IEEE/ASME Transactions on Mechatronics, 2024, 29(3):2196-2207.

[13] *Abe Ryo, Kanamori Chisato.,* Development of a Spherical Shell Robot with Rolling and Legged Locomotion, Journal of Robotics and Mechatronics, 2023, 35(2): 483-491.

[14] *Li chunying, Guo shuxiang*. Performance evaluation of spherical underwater robot with attitude controller, Ocean Engineering, 2023, 268(15).

[15] *Bo-han Xu, Fan Zhang, Li Zeng et al.* Research Progress on Key Technology of Spherical Joints. Micromotors, 2024, 57(2): 67-72.

[16] *Long Ma, Han-xu Sun, Jing-zhou Song et al.,* Adaptive control method for the high-speed linear motion of a spherical robot, Journal of Vibration and Shock, 2021, 40(6): 201-211.

[17] *An Ruochen, Guo Shuxiang, Zheng Liang et al.* Uncertain moving obstacles avoiding method in 3D arbitrary path planning for a spherical underwater robot. Robotics and Autonomous Systems, 2022, 151.

[18] *Montenegro Guelis, Chacon Roberto, Fabregas Ernesto et al.,* Modeling and Control of a Spherical Robot in the CoppeliaSim Simulator. Sensors, 2022, 22(16).

[19] *Haribabu S, Pathak PM.* Study of Drag Forces in Fluid-Filled Pipe Inspection Robot. Lecture Notes in Mechanical Engineering, 2024, 1:787-801.

[20] *Sparakos-Papastavridis Emmanouil, Dai Jian S.*, A Variable Impedance Scheme Based on Power-Shaping Signals and Partial Knowledge of Link-Side Dynamics for Flexible-Joint Robot Interaction and Tracking Control. IEEE/ASME Transactions on Mechatronics, 2024, 29(1):588-601.

[21] *Yang Long, Zhou Yulin, Ma Qiuming.* Statics Property Analyses of a Novel Spherical Parallel Humanoid Robotic Ankle Mechanism, China Mechanical Engineering, 2017, 28(7):835-841.

[22] *Qiang Wu*. Research on optimization design of mechanical system based on ADAMS. China Metalforming Equipment & Manufacturing Technology, 2024, 59(1): 43-46. DOI:10.16316/j.issn.1672-0121.2024.01.008.